doi: 10.1093/pasj/xxx000

arXiv:1605.03963v1 [astro-ph.GA] 12 May 2016

Gas-to-dust ratio in massive star-forming galaxies at $z \sim 1.4$

Akifumi SEKO[1], Kouji OHTA[1], Kiyoto YABE[2,3], Bunyo HATSUKADE[2], Yuya AONO[1] and Daisuke IONO[2,4]

[1]Department of Astronomy, Kyoto University, Kitashirakawa-Oiwake-Cho, Sakyo-ku, Kyoto 606-8502
[2]National Astronomical Observatory of Japan, 2-21-1 Osawa, Mitaka, Tokyo 181-8588
[3]Kavli Institute for the Physics and Mathematics of the Universe (Kavli IPMU, WPI), The University of Tokyo Institutes for Advanced Study, The University of Tokyo, Kashiwa, Chiba 277-8583, Japan
[4]The Graduate University for Advanced Studies (SOKENDAI), 2-21-1 Osawa, Mitaka, Tokyo 181-0015

*E-mail: seko@kusastro.kyoto-u.ac.jp

Received 2016 March 29; Accepted 2016 May 12

Abstract

We present results of ^{12}CO($J=2-1$) observations toward four massive star-forming galaxies at $z \sim 1.4$ with the Nobeyama 45 m radio telescope. The galaxies are detected with *Spitzer*/MIPS in 24 μm, *Herschel*/SPIRE in 250 μm, and 350 μm and they mostly reside in the main sequence. Their gas-phase metallicities derived with N2 method by using the Hα and [NII]λ 6584 emission lines are near the solar value. CO lines are detected toward three galaxies. The molecular gas masses obtained are $(9.6-35)\times10^{10}$ $M_\odot$ by adopting the Galactic CO-to-H_2 conversion factor and the CO(2-1)/CO(1-0) flux ratio of 3. The dust masses derived with the modified blackbody model (assuming the dust temperature of 35 K and the emissivity index of 1.5) are $(2.4-5.4)\times10^{8}$ $M_\odot$. The resulting gas-to-dust ratios (not accounting for HI mass) at $z \sim 1.4$ are 220-1450, which are several times larger than those in local star-forming galaxies. A dependence of the gas-to-dust ratio on the far-infrared luminosity density is not clearly seen.

Key words: galaxies: evolution — galaxies: high-redshift — galaxies: ISM

1 Introduction

The redshift around 2 is a crucial epoch to understand galaxy evolution. The star-formation rate (SFR) density peaked around this redshift (e.g., Hopkins & Beacom 2006; Madau & Dickinson 2014), i.e., galaxies are considered to evolve dramatically at this epoch. SFRs of most of star-forming galaxies correlate well with their stellar mass which makes a sequence in a diagram of stellar mass versus SFR. The sequence is called main sequence, and is seen at each redshift up to at least $z \sim 2.5$ (e.g., Noeske et al. 2007; Daddi et al. 2007; Rodighiero et al. 2010; Whitaker et al. 2012, 2014; Speagle et al. 2014). Since such galaxies are primary population among star-forming galaxies, it is important to unveil the nature of the interstellar medium (ISM) in main-sequence galaxies for the understanding of galaxy evolution.

The advent of high-sensitivity millimeter, sub-millimeter, and far-infrared telescopes enables us to investigate molecular gas and dust in the main sequence star-forming galaxies around $z \sim 2$ (e.g., Daddi et al. 2010; Genzel et al. 2010; Tacconi et al. 2010; Tacconi et al. 2013; Seko et al. 2016; Elbaz et al. 2011; Magdis et al. 2012; Magnelli et al. 2012; Magnelli et al. 2014). Recent studies of molecular gas in main sequence galaxies at $z=1-2.5$ showed the molecular gas mass and its fraction against stellar mass [$f_{\rm mol} = M_{\rm mol}/(M_{\rm mol}+M_*)$] were signif-

© 2014. Astronomical Society of Japan.

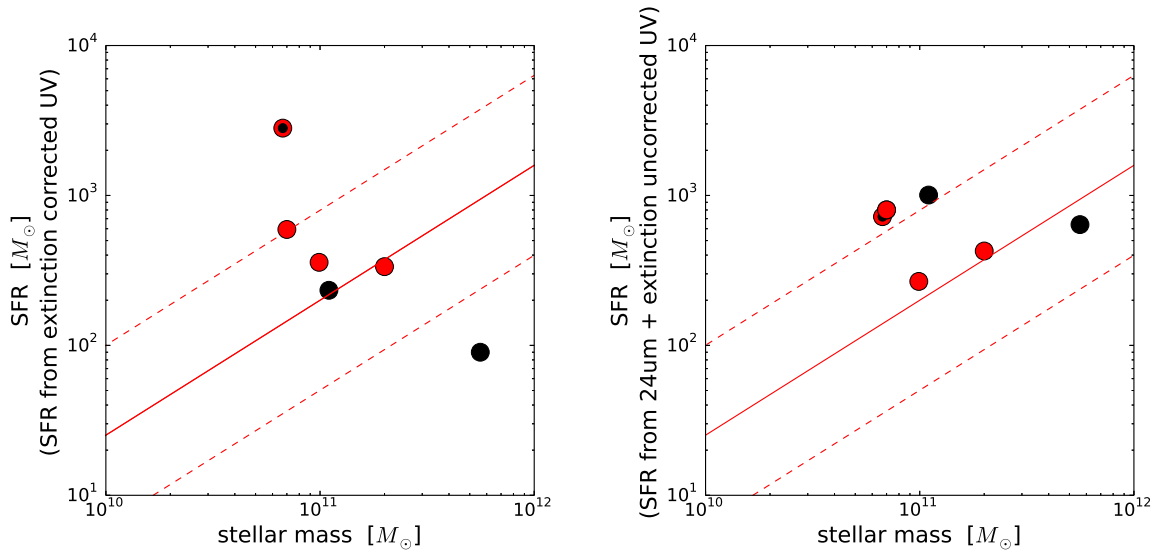

Fig. 1. Galaxy sample in the stellar mass−SFR diagram. SFRs are derived from extinction corrected UV luminosity densities (left), and sum of SFRs from 24 μm and SFRs from extinction uncorrected UV luminosity densities (right). Red and black filled circles show the galaxies in this study and Seko et al. (2014), respectively. Red circle with black circle refer to the COSMOS_9 which is one of the target galaxies in this study and Seko et al. (2014). Solid line represents main sequence by Daddi et al. (2010) derived for galaxies at $z \sim 2$. Dashed lines show the scatter of ± 0.6 dex.

icantly larger than those in local spiral galaxies (e.g., Daddi et al. 2010; Tacconi et al. 2010; Tacconi et al. 2013; Seko et al. 2016). The dust mass in main sequence galaxies at $z \sim 1-2$ was also found to be larger than that in the present-day spiral galaxies (e.g., Magdis et al. 2012; Magnelli et al. 2012; Seko et al. 2016).

The gas-to-dust ratio in galaxies is also an important parameter that is closely related to galaxy evolution. In the local universe, gas-to-dust ratio is ~ 150 at solar metallicity and depends on gas-phase metallicity; the ratio decreases with increasing metallicity (e.g., Leroy et al. 2011; Rémy-Ruyer et al. 2014). In the high redshift universe, the number of main-sequence galaxies observed with both CO and dust with known metallicities is still very limited. Saintonge et al. (2013) derived gas-to-dust ratios in lensed main-sequence galaxies at $z = 1.4-3.1$ from the CO and dust emissions detected with IRAM Plateau de Bure Interferometer and *Herschel*/PACS and SPIRE, respectively. The metallicities of their galaxy sample were mostly derived with the R23 (by using the Hβ, [OII]λ 3727, and [OIII]$\lambda\lambda$ 4959,5007 emission lines) or N2 (by using Hα, [NII]λ 6584) method. They showed the gas-to-dust ratio was about two times larger than that in local galaxies at a fixed metallicity. Seko et al. (2014) presented the results of CO observations of three massive star-forming galaxies at $z \sim 1.4$ detected with MIPS and SPIRE. Their metallicities derived using the N2 method were near the solar value. Although the CO emissions from each galaxy were not detected, the stacked CO profile shows the emission, and the molecular gas mass was derived. With the average dust mass, they showed the average gas-to-dust ratio was comparable to that in local galaxies with solar metallicity. By using ALMA, Seko et al. (2016) observed CO and dust emission of twenty main sequence galaxies with known metallicity at $z \sim 1.4$. Almost all of them are not detected in MIPS nor SPIRE. The result from the stacking analysis showed that the gas-to-dust ratio was $3-4$ times larger than that in local galaxies at a fixed metallicity. The gas-to-dust ratio may depend on the infrared flux (or luminosity). Therefore, we need to examine the gas-to-dust ratios in more galaxies detected in mid/far-infrared.

In this paper, we present ^{12}CO($J = 2-1$) observations of four massive star-forming galaxies with near solar metallicity at $z \sim 1.4$ which are detected with *Spiter*/MIPS in 24 μm, *Herschel*/SPIRE in 250 μm and 350 μm to study whether star-forming galaxies detected in mid/far-infrared wavelength show the similar gas-to-dust ratio in local galaxies. Sample selection and observations and data reductions are described in Section 2, and 3, respectively. We present the results, a discussion, and summary in section 4, section 5, and section 6, respectively. Throughout this paper, the Λ-CDM cosmology with $H_0 = 70$ km s^{-1} Mpc^{-1}, $\Omega_{\rm M} = 0.30$, and $\Omega_\Lambda = 0.70$ is adopted.

2 Sample

The galaxy sample was taken from Yabe et al. (2012, 2014) and Roseboom et al. (2012). They conducted near-infrared spectroscopic observations toward star-forming galaxies at $z \sim 1.4$ in the Subaru XMM/Newton Deep Survey (SXDS) field and in the Cosmological Evolution Survey (COSMOS) field, respectively, using Fiber Multi Object Spectrograph (FMOS) on the Subaru telescope. The galaxy sample by Yabe et al. (2012, 2014) con-

Table 1. Galaxy sample.

Source	RA (J2000.0)	Dec (J2000.0)	$z_{\rm spec}$	metallicity $[12+\log({\rm O/H})]$	M_* * ($M_\odot$)	SFR*, † ($M_\odot$ yr^{-1})	SFR*, ‡ ($M_\odot$ yr^{-1})
SXDS1_13015	$02^{\rm h}17^{\rm m}13\overset{\rm s}{.}63$	$-5°09'39\overset{''}{.}8$	1.451	$8.85^{+0.04}_{-0.04}$	2.0×10^{11}	335	426
COSMOS_9§	$10^{\rm h}00^{\rm m}08\overset{\rm s}{.}76$	$+2°19'02\overset{''}{.}3$	1.461	<8.68	6.7×10^{10}	2812	722
COSMOS_50	$10^{\rm h}01^{\rm m}40\overset{\rm s}{.}28$	$+2°33'30\overset{''}{.}9$	1.21	$8.84^{+0.11}_{-0.11}$	7.0×10^{10}	593	801
COSMOS_53	$10^{\rm h}01^{\rm m}36\overset{\rm s}{.}15$	$+2°20'04\overset{''}{.}3$	1.21	$8.68^{+0.11}_{-0.11}$	9.9×10^{10}	358	267
SXDS1_12778§	$02^{\rm h}19^{\rm m}09\overset{\rm s}{.}45$	$-5°09'49\overset{''}{.}0$	1.396	$8.66^{+0.09}_{-0.13}$	5.6×10^{11}	90	639
SXDS3_80799§	$02^{\rm h}17^{\rm m}30\overset{\rm s}{.}04$	$-5°24'31\overset{''}{.}6$	1.429	$8.66^{+0.02}_{-0.02}$	1.1×10^{11}	233	1006

* We adopted Salpeter IMF.
† SFRs are derived from extinction corrected UV luminosity densities.
‡ SFRs are calculated by summing the SFRs derived from 24 μm flux densities and derived from UV luminosity densities.
§ Galaxy sample in Seko et al. (2014). Since COSMOS_9 especially showed a signal-like feature, we try to detect the CO emission again.

sists of *K*-band selected galaxies that are mostly on the main sequence at $z_{\rm phot}\sim1.4$. On the other hand, the galaxy sample in Roseboom et al. (2012) consists of MIPS and SPIRE selected sources. The spectroscopic redshift was derived using Hα emission line. The gas phase metallicity was derived with N2 method by using the Hα and [NII]λ 6584 emission lines (Pettini & Pagel 2004). We selected the galaxies with the metallicity of $12+\log({\rm O/H})>8.6$ to reduce the uncertainty of CO-to-H_2 conversion factors.

In order to derive the far-infrared luminosity and the dust mass, we further required the galaxies are detected with MIPS in 24 μm, SPIRE in 250 μm and 350 μm. We selected sources that appear isolated in the 24 μm image, allowing us to obtain reliable flux density in mid/far-infrared. In fact, the contamination of target galaxies by adjacent sources in the images at 250 μm and 350 μm is not serious. For the galaxies in the SXDS field, MIPS data were taken from the DR2 version of *Spitzer* Public Legacy Survey of the UKIDSS (UKIRT Infrared Deep Sky Survey) Ultra Deep Survey (SpUDS: J. Dunlop et al. in preparation). SPIRE data were taken from the DR1 version of the Herschel Multi-tired Extragalactic Survey (HerMES: Oliver et al. 2012). Object detection and photometry were made with SExtractor (Bertin & Arnouts 1996). For the galaxies in the COSMOS field, the photometric data of MIPS and SPIRE were taken from Roseboom et al. (2012). We made SED from MIR to FIR, and derived $L_{\rm FIR}(8-1000\ \mu{\rm m})$ by fitting model SEDs of star-forming galaxies (Chary & Elbaz 2001).

Among these selected galaxies, we chose galaxies that are located around the main-sequence of star-forming galaxies (Daddi et al. 2010). For the galaxies in the SXDS field, the stellar mass and SFR were taken from Yabe et al. (2012, 2014); the stellar masses are derived by fitting the SED from far-UV to mid-IR data and SFRs are derived from the rest-frame UV luminosity densities corrected for the dust extinction estimated from the rest-frame UV-slope. For the galaxies in the COSMOS field, using the photometry data in Muzzin et al. (2013), we derived stellar mass and SFR with the same method as those in the SXDS field. We selected four galaxies and they are shown in Table 1 [1]. The properties in mid and far-infrared are also listed in Table 2. In Table 1, SFR derived from extinction corrected UV luminosity density and from the sum of the 24 μm luminosity density and extinction uncorrected UV luminosity density, and they are shown in left panel and right panel of Fig. 1, respectively (red circles). For the sample in this paper (except for COSMOS_9), the SFRs from 24 μm luminosity density and extinction uncorrected UV luminosity density are consistent with those from extinction corrected UV luminosity density. The sample by Seko et al. (2014) is also shown in Table 1 and 2 and Fig. 1 (black circles) together with the sample in this paper.

Table 2. Mid and far-infrared properties of galaxy sample.

Source	S_{24} (mJy)	S_{250} (mJy)	S_{350} (mJy)	$L_{\rm FIR}$ ($L_\odot$)
SXDS1_13015	0.32 ± 0.02	43 ± 8	44 ± 10	3.4×10^{12}
COSMOS_9	0.44 ± 0.01	26 ± 3	25 ± 3	4.2×10^{12}
COSMOS_50	0.76 ± 0.01	47 ± 3	34 ± 3	2.9×10^{12}
COSMOS_53	0.36 ± 0.01	26 ± 3	22 ± 3	1.1×10^{12}
SXDS1_12778	0.46 ± 0.02	45 ± 7	59 ± 8	3.8×10^{12}
SXDS3_80799	0.59 ± 0.02	54 ± 6	46 ± 5	5.9×10^{12}

3 CO(*J*=2-1) observations and data reduction

We made ^{12}CO($J=2-1$) line observations toward the four star-forming galaxies at $z\sim1.4$ on 2014 March 22nd, 23rd, 25th (COSMOS_9 and COSMOS_50), 2015 January 29th, 31st, and February 1st (COSMOS_53 and SXDS1_13015) using the Nobeyama 45 m telescope. The observing frequencies were 93.677 to 104.316 GHz calculated with spectroscopic redshifts derived from the near-infrared observations. We used the two-beam sideband-separating SIS receiver for z-machine with dual

[1] COSMOS_9 was already observed by Seko et al. (2014), but its spectrum only exhibited a tentative CO-detection. Thus, we decided to re-observe COSMOS_9. In Seko et al. (2014), the stellar mass and SFR of COSMOS_9 were taken from Whitaker et al. (2011). The stellar mass and SFR are 3.7 times larger and 2.3 times smaller than those in this paper, respectively.

polarization (TZ; Nakajima et al. 2013). The half power beam width at these frequencies was $\sim$17 arcsec. We used the flexible FX-type spectrometer (spectral analysis machine for the 45 m telescope (SAM45); Iono et al. 2012). We can use up to 16 spectral windows (SPWs) and choose a band width of each SPW from several modes between 16 MHz and 2 GHz. To cover the wider range of velocity, we selected the 2 GHz mode. The frequency width of one channel is 488.28 kHz, because each array has 4096 channels. The image rejection ratios in the observing frequency ranges exceeded 10 dB. The system noise temperature ($T_{\rm sys}$) was typically 130-170 K. The accuracy of telescope pointing was checked every 50 min with the observations of SiO maser sources (o Cet and R Leo) near the galaxy sample. During the observations, the accuracy was within 3 arcsec.

We used the NEWSTAR software for the data reduction. The data taken under the condition of a wind speed of less than $5\ {\rm m\ s^{-1}}$ were used. In addition, we flagged data with poor baseline by visual inspection. Three persons independently set three criteria for the flagging to check the robustness of the results. All analyses showed similar results. After flagging, the effective integration time per galaxy was 4.2-8.8 hours. All data were converted from the antenna temperature ($T_{\rm A}$) to main beam temperature ($T_{\rm mb}$). The main beam efficiencies were 0.38 for COSMOS_9 and COSMOS_50 and of 0.42 for COSMOS_53 and SXDS1_13015 [2]. The root mean square noise temperature in $T_{\rm mb}$ scale was 0.7-1.5 mK.

4 Results

4.1 CO(2-1) spectra

The spectra obtained are shown in Fig. 2. The CO$(2-1)$ emission line was detected toward SXDS1_13015, COSMOS_50, and COSMOS_53 but was not detected toward COSMOS_9. The spectrum of SXDS1_13015 shows velocity width of $500\ {\rm km\ s^{-1}}$, and the noise level at a velocity resolution of $500\ {\rm km\ s^{-1}}$ (σ_{500}) is 0.41 mK. The signal-to-noise ratio (S/N) of SXDS1_13015 at the $500\ {\rm km\ s^{-1}}$ resolution is 4.1. The spectrum of COSMOS_50 shows a velocity width of 300 ${\rm km\ s^{-1}}$, and the noise level at the velocity resolution (σ_{300}) is 0.35 mK. The S/N of COSMOS_50 at the $300\ {\rm km\ s^{-1}}$ resolution is 4.6. The spectrum of COSMOS_53 shows a velocity width of $1000\ {\rm km\ s^{-1}}$, and the noise level at the velocity resolution (σ_{1000}) is 0.16 mK. The S/N of COSMOS_53 at the $1000\ {\rm km\ s^{-1}}$ resolution is 10.5. The velocity width is larger than a typical value ($\sim 200\ {\rm km\ s^{-1}}$) in main sequence galaxies at a similar redshift (e.g., Tacconi et al. 2013; Seko et al. 2016). We checked an I_{F814W}-band image taken with the Advanced Camera for Surveys (ACS) on the *Hubble Space Telescope* (Koekemoer et al. 2007). The image of COSMOS_53 shows that the target may be a merging system, thus the CO emission line may include both merging galaxies.

[2] If we adopted an aperture efficiency of 0.26 for COSMOS_9/COSMOS_50 and 0.27 for COSMOS_53/SXDS1_13015, their molecular gas masses and gas-to-dust ratios are 1.5 and 1.6 larger than those estimates with the main beam efficiency, respectively.

4.2 Molecular gas mass

We calculated the CO$(1-0)$ luminosity ($L^{'}_{\rm CO(1-0)}$) from the obtained spectrum with the following equation:

$$L^{'}_{\rm CO(1-0)} = 3.25\times10^{7}\ S_{\rm CO(2-1)}\Delta v R_{21}^{-1}\nu_{\rm rest(1-0)}^{-2} D_L^2 (1+z)^{-1}, \quad (1)$$

where $L^{'}_{\rm CO(1-0)}$ is measured in ${\rm K\ km\ s^{-1}\ pc^2}$, $S_{\rm CO(2-1)}$ is the observed CO$(2-1)$ flux density in Jy, Δv is the velocity width in ${\rm km\ s^{-1}}$, R_{21} is the flux ratio of CO$(2-1)$ to CO$(1-0)$, $\nu_{\rm rest(1-0)}$ is the rest frequency of the CO(1-0) emission line in GHz, and D_L is the luminosity distance in Mpc. The values of Δv for SXDS1_13015, COSMOS_50, and COSMOS_53 are $500\ {\rm km\ s^{-1}}$, $300\ {\rm km\ s^{-1}}$, and $1000\ {\rm km\ s^{-1}}$, respectively. The value of R_{21} is assumed to be 3, which is a typical value for color selected star-forming galaxies at $z=1-3$ (Carilli & Walter 2013; Daddi et al. 2015). For COSMOS_9, we derived the $2\sigma_{250}$ upper limit of the CO$(1-0)$ luminosity (σ_{250} is a noise level at a 250 ${\rm km\ s^{-1}}$ velocity resolution) assuming a velocity width of $250\ {\rm km\ s^{-1}}$, as in Seko et al. (2014). The derived CO$(1-0)$ luminosities of the galaxies are shown in Table 3.

Then, we derived the molecular gas mass by using the CO-to-H_2 conversion factor ($\alpha_{\rm CO}$). The $\alpha_{\rm CO}$ correlates with metallicity in local star-forming galaxies; the value of $\alpha_{\rm CO}$ is smaller in galaxies with higher metallicity (e.g., Arimoto et al. 1996; Leroy et al. 2011). According to recent studies, a similar relation is seen in star-forming galaxies at $z=1-2$ (Genzel et al. 2012), and $\alpha_{\rm CO}$ is close to the Galactic value for the main sequence star-forming galaxies with solar metallicity (e.g., Daddi et al. 2010; Genzel et al. 2012). The uncertainty in $\alpha_{\rm CO}$ is smaller than that at lower metallicity. Since the galaxies selected have metallicity close to the solar metallicity, we adopt the Galactic $\alpha_{\rm CO}$ value of $4.36\ M_\odot\ ({\rm K\ km\ s^{-1}\ pc^2})^{-1}$ (including helium mass). For COSMOS_53, since it is possible that this galaxy is undergoing a merging, we also derived the molecular gas mass adopting the ULIRG-like conversion factor ($0.8\ M_\odot\ ({\rm K\ km\ s^{-1}\ pc^2})^{-1}$; Downes & Solomon 1998). The resulting molecular gas masses except for COSMOS_9 are $(1-3.5)\times10^{11}\ M_\odot$ as given in Table 3. The uncertainty given to the molecular gas mass is based on SN of the spectrum and does not include the uncertainty of the luminosity ratio and $\alpha_{\rm CO}$. The fractions of molecular gas against stellar mass are 0.5-0.8 (for COSMOS_53, $f_{\rm mol}=0.4$ with the ULIRG-like conversion factor). These values are in agreement with those in the previous studies (e.g., Daddi et al. 2010; Tacconi et al. 2010; Tacconi et al. 2013; Seko et al. 2016).

Table 3. Molecular gas and dust properties of galaxy sample.

Source	$L'_{\rm CO(1-0)}$ (K km s^{-1} pc^2)	$M_{\rm mol}{}^*$ ($M_\odot$)	$f_{\rm mol}$	$M_{\rm d}$ ($M_\odot$)	Gas-to-dust ratio
SXDS1_13015	$(5.4\pm1.3)\times10^{10}$	$(2.4\pm0.6)\times10^{11}$	0.54 ± 0.07	5.4×10^8	440 ± 110
COSMOS_9	$<2.2\times10^{10}$	$<9.7\times10^{10}$	<0.59	3.4×10^8	<290
COSMOS_50	$(2.2\pm0.5)\times10^{10}$	$(9.6\pm2.1)\times10^{10}$	0.58 ± 0.07	4.5×10^8	220 ± 50
COSMOS_53	$(8.1\pm0.8)\times10^{10}$	$(3.5\pm0.3)\times10^{11}$	0.78 ± 0.02	2.4×10^8	1450 ± 140
		$(6.5\pm0.6)\times10^{10\dagger}$	$0.40\pm0.01^\dagger$		$265\pm25^\dagger$
SXDS1_12778	$<2.9\times10^{10}$	$<1.3\times10^{11}$	<0.19	5.4×10^8	<240
SXDS3_80799	$<2.2\times10^{10}$	$<9.7\times10^{10}$	<0.47	6.7×10^8	<150

* We adopted $\alpha_{\rm CO}=4.36\ M_\odot\ ({\rm K\ km\ s^{-1}\ pc^2})^{-1}$.
† We adopted $\alpha_{\rm CO}=0.8\ M_\odot\ ({\rm K\ km\ s^{-1}\ pc^2})^{-1}$.

4.3 Dust mass

The dust mass is derived from

$$M_{\rm d}=\frac{S_{\rm obs}D_L^2}{(1+z)\kappa_{\rm d}(\nu_{\rm rest})B(\nu_{\rm rest},T_{\rm d})}, \quad (2)$$

where $S_{\rm obs}$ is the observed flux density, $\kappa_{\rm d}(\nu_{\rm rest})$ is the dust mass absorption coefficient in the rest-frame frequency, $T_{\rm d}$ is the dust temperature, and $B(\nu_{\rm rest},T_{\rm d})$ is the Planck function. $\kappa_{\rm d}$ varies with frequency as $\kappa_{\rm d}\propto\nu^\beta$, where β is the dust emissivity index. As in Seko et al. (2014), we used a 250 μm flux density for $S_{\rm obs}$, $\kappa_{\rm d}(125\ \mu{\rm m})=1.875\ {\rm m^2\ kg^{-1}}$ (Hildebrand 1983), $\beta=1.5$, and $T_{\rm d}=35$ K. Since our galaxy sample tends to be located in the upper part of the main sequence, we adopted a typical dust temperature for galaxies with higher specific SFRs among main sequence galaxies (Magnelli et al. 2014). The dust mass can change by a factor of $\sim$1.8 when we adopt dust temperatures of 30 or 40 K. The uncertainty arisen from β is 10 % in adopting $\beta=$1.0 or 2.0, since we use the flux density at the rest-wavelength of 105 μm and we use $\kappa_{\rm d}$ at 125 μm. The resulting dust masses are $(2.4-5.4)\times10^8\ M_\odot$ as given in Table 3.

4.4 Gas-to-dust ratio

We calculated gas-to-dust ratios ($M_{\rm mol}/M_{\rm dust}$) of the galaxy sample. The resulting gas-to-dust ratios are $220-1450$ as shown in Table 3 and plotted against the gas metallicity with red circles and the arrow (upper limit) in the left panel of Fig. 3. For COSMOS_53, the gas-to-dust ratio is 265 (open red circle), when we use the ULIRG-like CO-to-H_2 conversion factor. Note that the gas-to-dust ratio does not include the mass of the atomic hydrogen gas (HI). According to a semi-empirical model by Popping et al. (2015), HI mass in galaxies at $z\sim1.4$ with halo mass of $10^{12-14}\ M_\odot$ is half or comparable to the H_2 mass. Therefore, the actual gas-to-dust ratios may be larger by 0.2-0.3 dex.

5 Discussion

In the left panel of Fig. 3, we also plot the upper limits of the gas-to-dust ratio at $z\sim1.4$ by Seko et al. (2014) (SXDS1_12778 and SXDS3_80799) with black arrows. The star-forming galaxies with solar metallicity detected with mid/far-infrared (MIPS and SPIRE) show various gas-to-dust ratios. The ratios in local galaxies (including HI mass) are also shown with cyan diamonds (Leroy et al. 2011) and squares (Rémy-Ruyer et al. 2014). The ratios in SXDS1_13015, COSMOS_50, and COSMOS_53 (even if we use the ULIRG-like CO-to-H_2 conversion factor for COSMOS_53) are several times larger than those in local galaxies with solar metallicity. While dust masses are derived from the modified blackbody model in this study, if we adopt the dust model by Draine & Li (2007) (hereafter DL07 model), the dust mass is systematically 2-3 times larger than that derived from the modified blackbody (e.g., Magdis et al. 2012; Magnelli et al. 2012). If we used the DL07 model for deriving dust mass, our results can shift to near the local values. As mentioned above, if the HI mass is included, the gas-to-dust ratio at $z\sim$1.4 is still larger than that in the local universe.

Seko et al. (2016) conducted observations of ^{12}CO($J=5-4$) emission line and dust continuum emission toward twenty star-forming galaxies at $z\sim1.4$ with wider range of stellar mass and metallicity by using ALMA. Almost all of their galaxies were not detected with MIPS nor SPIRE. They found that the gas-to-dust ratio in main sequence galaxies at $z\sim1.4$ is 3-4 times larger than that in local galaxies at each fixed metallicity. In the left panel of Fig. 3, the result of stacking analysis by Seko et al. (2016) is plotted with green stars. They adopted the metallicity-dependent CO-to-H_2 conversion factor by Genzel et al. (2012). In addition, they assumed $T_{\rm d}=30$ K, because their galaxies are located around the center of main sequence by Daddi et al. (2010). If $T_{\rm d}=35$ K is assumed, the gas-to-dust ratios in Seko et al. (2016) is larger than those with $T_{\rm d}=30$ K by ~0.1 dex. Results in this study are roughly consistent with those by Seko et al. (2016). One galaxy, SXDS1_13015, was also observed by Seko et al. (2016). By adopting the same conversion factor and dust temperature in

this paper, the gas-to-dust ratio derived by Seko et al. (2016) ($\sim$470; $M_{\rm mol} = 1.8 \times 10^{11}\ M_\odot$ and $M_{\rm dust} = 3.8 \times 10^{8}\ M_\odot$) is in agreement with that obtained in this paper.

To examine the dependence of gas-to-dust ratio on far-infrared luminosity density, we plot the gas-to-dust ratios in the star-forming galaxies with solar metallicity ($12 + \log({\rm O/H}) > 8.6$) in this study and those by the previous studies (Seko et al. 2014, 2016) against the rest-frame luminosity density at 0.5 mm ($L_{\rm rest\ 0.5\ mm}$; right panel of Fig. 3). Although it may be better to see the dependence on the total infrared luminosity rather than the luminosity density, since we only have the flux densities in the band-6 for almost all of the ALMA sample and the total luminosity depends on the SED, we use the $L_{\rm rest\ 0.5\ mm}$ to avoid the uncertainty. The luminosity densities of the galaxies in this study and Seko et al. (2014) are estimated from the best fitted model SED by Chary & Elbaz (2001). The gas-to-dust ratio does not seem to depend on the luminosity density at $0.5\ {\rm mm}$. Although most of the ratios are 200-500 (if we use the ULIRG-like conversion factor for COSMOS_53), the lower and upper limits indicate that star-forming galaxies with solar metallicity at $z \sim 1.4$ probe a wide range of gas-to-dust ratios.

6 Summary

We carried out $^{12}{\rm CO}(J = 2-1)$ observations toward four massive star-forming galaxies at $z \sim 1.4$ around the main sequence with the Nobeyama 45 m radio telescope. The galaxies were detected with *Spitzer*/MIPS in 24 μm and *Herschel*/SPIRE in 250 μm, and 350 μm. The metallicities of these galaxies which were derived with N2 method were near the solar value. CO emission lines were detected toward three of the galaxies. The masses of molecular gas are $(9.6-35) \times 10^{10}\ M_\odot$ by adopting the Galactic CO-to-H_2 conversion factor and the CO(2-1)/CO(1-0) flux ratio of 3. The masses of dust are $(2.4-5.4) \times 10^{8}\ M_\odot$ with the modified blackbody model by assuming $T_{\rm dust} = 35$ K and $\beta = 1.5$. The resulting gas-to-dust ratios (not accounting for HI) are $220-1450$. Most of them are several times larger than those in local galaxies with solar metallicity. The dependence of the gas-to-dust ratio on the far-infrared luminosity density is not clearly seen, even if we include the galaxy sample in Seko et al. (2016) whose luminosity density is smaller than those of the galaxy sample in this paper.

Acknowledgments

We would like to thank the referee for useful comments and suggestions. We acknowledge the members of Nobeyama Radio Observatory for their help during the observations. A.S. is supported by Research Fellowship for Young Scientists from the Japan Society of the Promotion of Science (JSPS). K.O. was supported by Grant-in-Aid for Scientific Research (C) (24540230) from JSPS. Kavli IPMU is supported by World Premier International Research Center Initiative (WPI), MEXT, Japan.

References

Arimoto, N., Sofue, Y., & Tsujimoto, T. 1996, PASJ, 48, 275
Bertin, E., & Arnouts, S. 1996, A&AS, 117, 393
Carilli, C. L., & Walter, F. 2013, ARA&A, 51, 105
Chary, R., & Elbaz, D. 2001, ApJ, 556, 562
Daddi, E., et al. 2007, ApJ, 670, 156
Daddi, E., et al. 2010, ApJ, 713, 686
Daddi, E., et al. 2015, A&A, 577, A46
Downes, D., & Solomon, P. M. 1998, ApJ, 507, 615
Draine, B. T., & Li, A. 2007, ApJ, 657, 810
Elbaz, D., et al. 2011, A&A, 533, A119
Genzel, R., et al. 2012, ApJ, 746, 69
Genzel, R., et al. 2010, MNRAS, 407, 2091
Hildebrand, R. H. 1983, QJRAS, 24, 267
Hopkins, A. M., & Beacom, J. F. 2006, ApJ, 651, 142
Iono, D., et al. 2012, PASJ, 64, L2
Koekemoer, A. M., et al. 2007, ApJS, 172, 196
Leroy, A. K., et al. 2011, ApJ, 737, 12
Madau, P., & Dickinson, M. 2014, ARA&A, 52, 415
Magdis, G. E., et al. 2012, ApJ, 760, 6
Magnelli, B., et al. 2014, A&A, 561, A86
Magnelli, B., et al. 2012, A&A, 548, A22
Muzzin, A., et al. 2013, ApJS, 206, 8
Nakajima, T. et al. 2013, PASP, 125, 252
Noeske, K. G., et al. 2007, ApJL, 660, L43
Oliver, S. J., et al. 2012, MNRAS, 424, 1614
Pettini, M., & Pagel, B. E. J. 2004, MNRAS, 348, L59
Popping, G., Behroozi, P. S., & Peeples, M. S. 2015, MNRAS, 449, 477
Rémy-Ruyer, A., et al. 2014, A&A, 563, A31
Rodighiero, G., et al. 2010, A&A, 518, L25
Roseboom, I. G., et al. 2012, MNRAS, 426, 1782
Saintonge, A., et al. 2013, ApJ, 778, 2
Seko, A., Ohta, K., Hatsukade, B., Yabe, K., Takeuchi, T., & Iono, D. 2014, PASJ, 66, 81
Seko, A., Ohta, K., Yabe, K., Hatsukade, B., Akiyama, M., Iwamuro, F., Tamura, N., & Dalton, G. 2016, ApJ, 819, 82
Speagle, J. S., Steinhardt, C. L., Capak, P. L., & Silverman, J. D. 2014, ApJS, 214, 15
Tacconi, L. J., et al. 2010, Nature, 463, 781
Tacconi, L. J., et al. 2013, ApJ, 768, 74
Whitaker, K. E., et al. 2011, ApJ, 735, 86
Whitaker, K. E., van Dokkum, P. G., Brammer, G., & Franx, M. 2012, ApJL, 754, L29
Whitaker, K. E., et al. 2014, ApJ, 795, 104
Yabe, K., et al. 2012, PASJ, 64, 60
Yabe, K., et al. 2014, MNRAS, 437, 3647

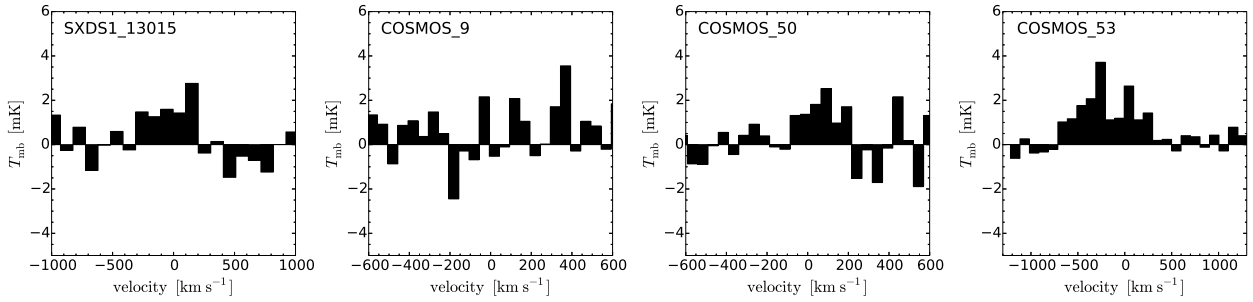

Fig. 2. CO$(2-1)$ spectra of SXDS1_13015 (left), COSMOS_9 (center left), COSMOS_50 (center right), and COSMOS_53 (right) taken with the Nobeyama 45 m telescope. Spectra are binned with a 50 km s^{-1} velocity width for COSMOS_9 and COSMOS_50, with a 100 km s^{-1} velocity width for COSMOS_53 and SXDS1_13015. The zero velocity is derived by referring the spectroscopic redshift by Hα observation.

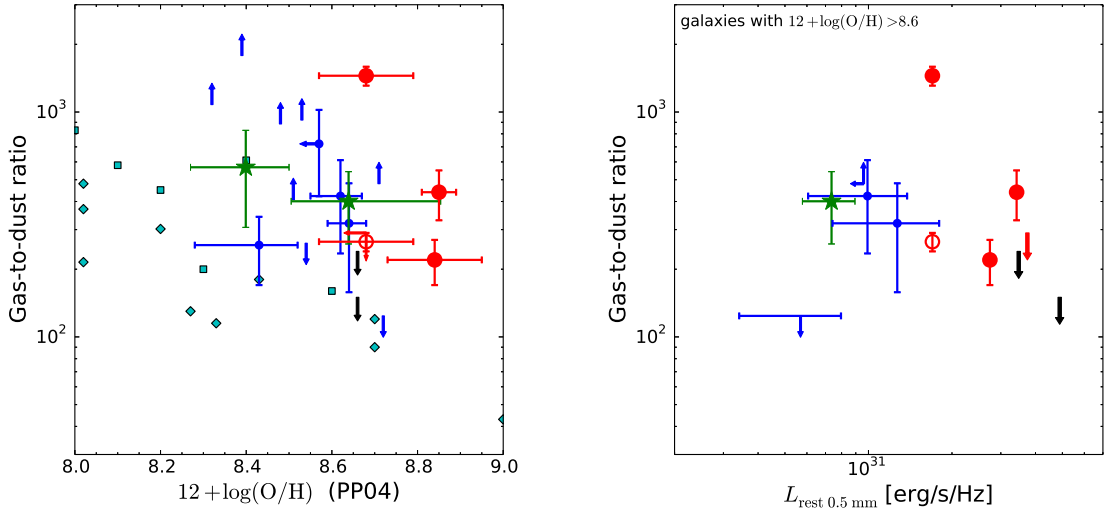

Fig. 3. Gas-to-dust ratio against metallicity (left), and luminosity density at rest-wavelength of 0.5 mm for galaxies with $12+\log({\rm O/H})>8.6$ (right). Red and black symbols refer to the galaxies in this paper and in Seko et al. (2014), respectively. Open circle represents COSMOS_53 with the ULIRG-like $\alpha_{\rm CO}$. Blue filled circles refer to the individual galaxies and green stars refer to the results of metallicity-based stacking analysis by Seko et al. (2016). Cyan diamonds represent local galaxies by Leroy et al. (2011) and cyan squares represent the average values in local galaxies shown by Rémy-Ruyer et al. (2014). (Metallicities are calibrated using Pettini & Pagel 2004.)